1   Sensors

Sensors are the sensitive part of the pixel detector for charged particle detection functioning as a solid-state ionization chamber. The sensor has to meet considerable geometrical constraints concerning its thickness and granularity as well as a high charge collection efficiency within the sensitive volume, while sustaining a massive amount of ionizing and non-ionizing particle radiation damage. This is reflected on one hand in the selection of the bulk material and on the other hand with the design of the pixel structure itself.

1.1   Design

The ATLAS pixel sensor is an array of bipolar diodes on a high resistivity bulk close to intrinsic charge concentration by implanting high positive (p^+) and negative (n^+) dose regions on one wafer surface each. An asymmetric depletion region on the p^+-n junction can be operated in reverse bias and extends over the whole sensor bulk volume, able to collect and thus detect all charges produced in the volume by ionizing particles. The sensor concept guarantees inter pixel isolation, minimizes leakage current and makes the sensor testable as well as tolerant to radiation damage.

The pixel sensor consist of $250\,\mu$m thick n bulk with n^+ implants on the read-out side and the p-n junction on the back side. Aside from increased leakage current, radiation damage will invert the sensor bulk and then gradually increase the depletion voltage. For unirradiated sensors the depletion starts at the back (p) side and the pixels are not isolated from each other until full depletion of the bulk. Irradiation of the bulk leads to a change of the effective doping concentration N_{eff}: first N_{eff} drops and then runs through type inversion with increasing N_{eff} afterwards [4]. At the point of type inversion the junction moves to the front (n) side isolating the pixels and enabling operation even if the bulk cannot be fully depleted. Maximum achievable depletion is still desirable to maximize the signal. The advantage of the depletion zone for the n^+-in-n design is shown in Figure 1.
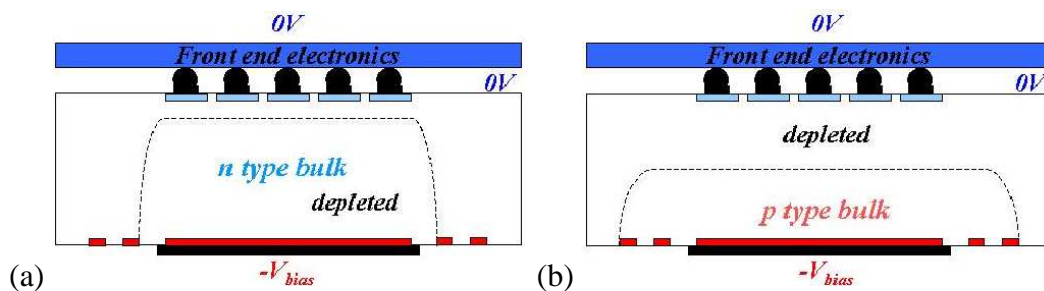

Figure 1: Comparison of depletion zones in n^+-in-n pixel sensors before (a) and after (b) type inversion. After type inversion the depletion zone grows from the pixel side and allows operation even if the bulk is not fully depleted

Oxygen impurities in the bulk ensure high tolerance of silicon against bulk damage caused by charged hadrons [1]. A comparison of the evolution of charge densities in standard and oxygenated silicon during irradiation with hadrons is shown in Figure 2a. Besides the continuous

irradiation of the sensors during beam time the induced doping concentration N_{eff} evolves due to thermal effects: On short time scales N_{eff} drops (beneficial annealing), runs then through a minimum of constant damage and finally on longer time scales increases again, (reverse annealing, see Figure 2b).

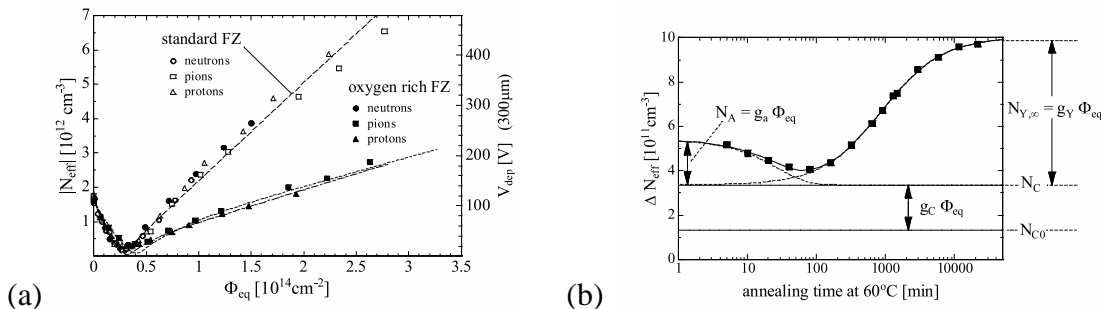(a)   (b)

Figure 2: (a) Evolution of effective charge densities and full depletion voltage in standard and oxygenated silicon during irradiation with hadrons. In oxygenated silicon the increase after type inversion is significantly lower. (b) Evolution of the effective doping concentration due to annealing and reverse annealing effects. The parameterization of this evolution is the so-called "Hamburg model" and represents an important input of ATLAS pixel sensors which should be operated near the point of minimal depletion voltages. In oxygenated silicon, both N_C and N_Y are reduced [1]

While the beneficial annealing is not altered in oxygenated silicon, both the constant radiation damange (N_C) is reduced and the reverse annealing (N_Y, see Figure 2b) is significantly slowed down [1] producing a lower overall effective charge density in similarly irradiated samples after identical annealing scenarios. Sensors built from such material exhibit deeper depletion zones at the same bias voltage and full depletion at a lower bias voltage.

By choosing an appropriate temperature profile (i.e. operation at 0°C, short periods of +20°C during detector access, cooling down to some −20°C during longer operation breaks of the experiment) one tries to keep sensors near the lowest possible N_{eff} near the constant damage to benefit from the lowest possible depletion voltage. Model calculations (Figure 3) of the combined effects of bulk irradiation and annealing have been performed and published in [3]. The radiation induced increase of the intrinsic charge carrier concentration leads to higher leakage currents and contributes to noise also. Here, cooling of the sensors to values well below room temperature helps to reduce these effects.

The positive and the negative implanted wafer sides are both structured by mask processes for implantation, metallization and deposition of silicon oxide and nitrite. This double sided processing demands precise mask steps and incorporates front-to-back mask alignment in the order of a few micrometer. However, this allows for a segmented n$^+$ implantation used for definition of pixel cells and a guard ring structure on the p$^+$ implanted wafer side, locating the main voltage drop on the sensor surface opposite to the bump connections. The 250 μm thick high resistivity silicon bulk of 2 to 3 kΩ/cm can be easily fully depleted before type inversion with bias voltages below 100 V. After type inversion the depletion zone grows primarily from the segmented n$^+$ implantation as the region of highest electric field into the bulk now converted to p-type.
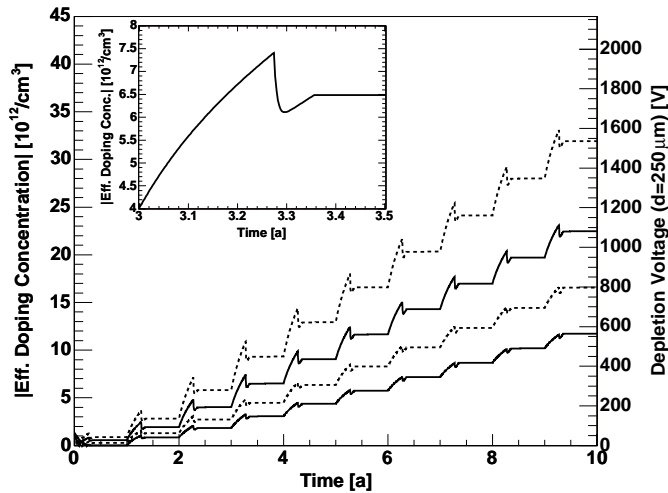
Figure 3: Change of the effective doping concentration (left scale) and the voltage necessary for full depletion (right scale) of sensors according to irradiation and annealing effects under the Hamburg model for the two inner pixel detector layers in a standard (solid) and elevated (dashed) radiation scenario

On the sensor front side pixel structures are arranged and isolated by moderated p-spray implantations which have been proven to be radiation tolerant with respect to surface damages induced by ionising charged particles for doses up to 50 Mrad in silicon. Its principal layout is shown in Figure 4a. The p-spray dose is regulated in an additional mask step, creating a slightly deeper high dose p-spray region in the center of the inter pixel gap and a slightly shallower low dose layer everywhere else. This isolation technique avoids high field regions in the interface between pixel, isolation and bulk and ensures the radiation tolerance of the design [5, 6]

All 46080 read-out channels of an entire sensor tile are connected to a common bias grid structure (Figure 4b) employing a punch-through connection technique to each channel what allows to bias the whole sensor easily without individual connections. This bias grid is beeing used for quality assurance measurements before any read-out electronics is connected to sensors. An opening for each pixel in the passivation layer of the sensor allows to connect each channel using a bump-bond technique to front-end electronics, which is DC coupled and provides biasing of each individual pixel.

1.2 Prototyping and tests

Extensively bulk and surface design features of the sensors have electrically been tested during the prototyping [7] and a dedicated pixel sensor quality assurance plan has been developed [8]. Sensor layout has been designed on four inch double side wafers, which include three sensor tiles of about 18 mm × 62 mm each. During the prototyping dedicated test structures have been developed which were placed on the ATLAS pixel sensor wafer around the sensor tiles allowing dedicated electrical tests of design features of the sensor (Figure 5).

The quality control included mechanical as well as electrial inspections and tests. Examples of visual and mechanics tests are scratch pattern marking and wafer identification, visual
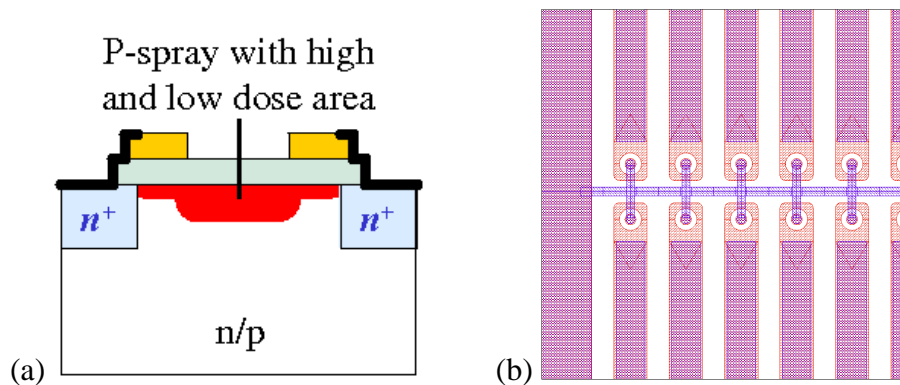
(a) (b)

Figure 4: (a) Principal layout of the moderated p-spray isolation which consist of high and low dose areas between n^+ pixel implantions in the n bulk. Compared to other isolation profiles like p-stop and p-spray high field regions are avoided in the transition regions between pixel and bulk. (b) Layout detail of the bias grid visible in the production mask for a pixel double row
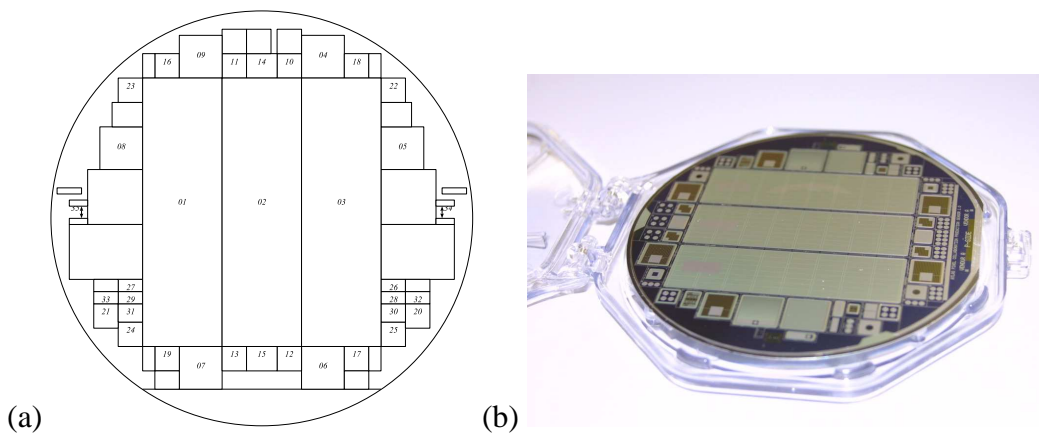

(a) (b)

Figure 5: (a) Geometrical layout of the sensor wafer. Central large structures 01, 02 and 03 are the sensor tiles carrying 46080 read-out channels employed in ATLAS pixel sensor modules, structures 04 to 35 are dedicated test structures to monitor the quality of prototyping and production. (b) A pictural view of the 4 inch ATLAS pixel sensor wafer (p-side view)
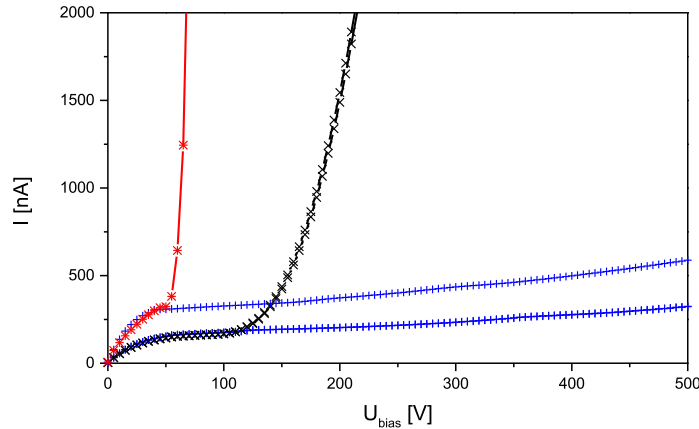
Figure 6: Examples of dark current vs. bias voltage curves on pre-series sensors tiles. While the two blue curves are examples of practically perfect diodes the black curve shows an break down between 150 and 200 V and the red curve shows a very steep break down behaviour near the typical depletion voltage indicated a defect on the n-side of the sensor

inspection of the surface quality, planarity and thickness measurements of wafers. Electrical tests included the measurement of the leakage current and the capacitance of diodes with guard ring structure. Leakage current was monitored on sensor tiles, single and mini chips, current and capacitance measurements were performed on oxide structures.

As an example of the bulk characteristics the dark current on sensor tiles is monitored. The break down voltage has to be well above 150 V. Figure 6 shows an example of measurements performed during the prototyping. While the two blue curves are examples of practically perfect diodes the black curve shows a break down between 150 and 200 V and the red curve shows a very steep break down behaviour near the typical depletion voltage indicating a defect on the n-side of the sensor.

As the moderated p-spray dose is one of the critical issues of the sensor design the measurement of the p-spray dose is one important quality control test. There, a dedicated punch through structure as well as an oxide structure is needed to determine the oxide capacitance. An example of a punch through measurement is shown in Figure 7. The idea of this measurement is to determine the current I between an individual pixel and the bias grid (Figure 7c) as a function of the potential difference ΔU while the sensor bulk is biased at -150 V. The resulting current (Figure 7d) increases for good isolations at $\Delta U > 1$ V. This together with the oxide measurement (not shown here) leads to the p-spray dose [8]. This example shows the necessity of advanced quality control measurements to assure the radiation hardness of production sensors. Some of the sensors had to be recjected due to this criteria during the production process.

(a)

(b)

bias dots on
grid contact

n-side pixel contact

joined pixel implantation

n-Substrate

high dose p-spray

p+ contact
implantation

p-side contact

(c)

(d)

ground

n^+ pixel
implantation

$-\Delta V$

n^+ bias
structure

I

n-type bulk

p-spray

p^+

operation voltage -150V

vendor A punch through structures

vendor B punch through structures

from middle pre-series   from later production runs

I_{sd} [nA]

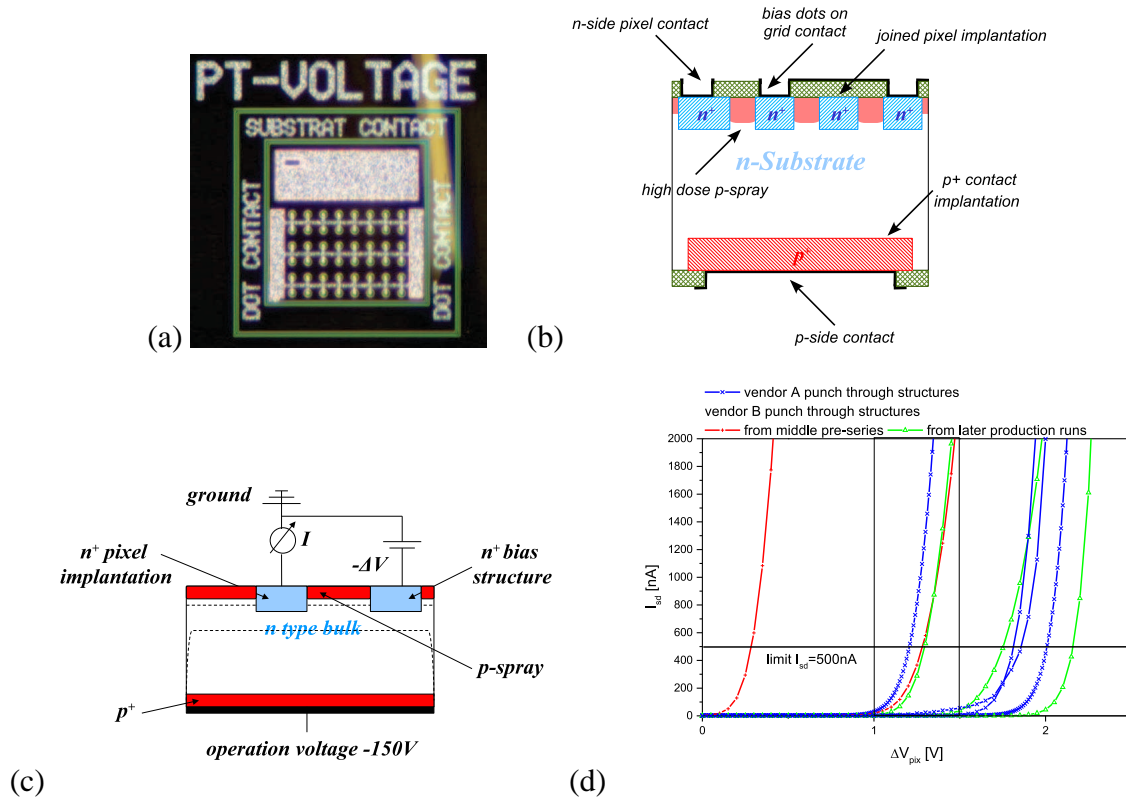ΔV_{pix} [V]

limit I_{sd}=500nA

Figure 7: (a) Punch through test device with 48 bias dot implantations and the reflection of a probe needle to the right. (b) Cut-away view of a punch through test device. (c) Electrical set-up to monitor the bias dot current vs. the potential difference test on depleted substrate. (d) Example of the punch through current measurement on several prototyping structures at the nominal bias voltage of 150 V. The left red curve is an example of a too low potential difference which occured during the prototyping compared to later productions which fulfilled the isolation criteria of more than 1 V
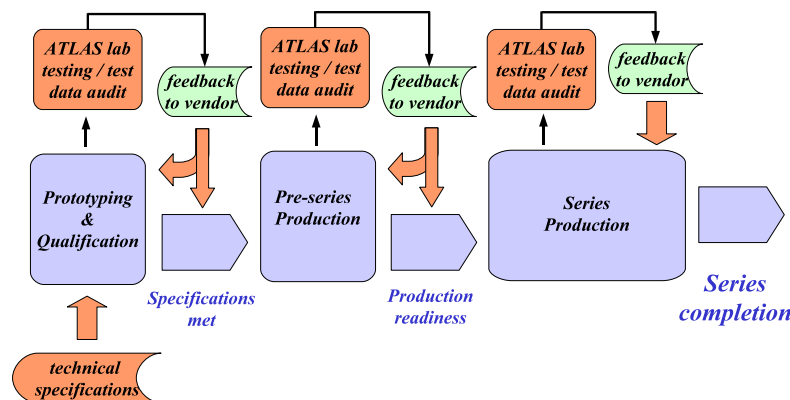
Figure 8: Information feedback for the sensor quality optimization during the various production steps of ATLAS pixel sensor wafers

1.3   Production and quality assurance

Sensor tiles have been produced with two independent vendors, which went through the prototyping and qualification process. Based on the experience during the prototyping specialized quality assurance procedures have been employed for the series production of sensors [9, 10] and were carried out as collaborative effort at four different pixel sensor institutes. Extensive cross calibration of mechanical and electrical measurements was performed during these processes. The schematical layout of the information feedback between sensor institutes and vendors during the various production steps are scetched in Figure 8.

The progress of the production of ATLAS pixel sensors is shown in Figure 9. More than 2200 sensors went successfully through the quality assurance process and have been made available for hybridisation [11] to the front-end electronics.

References

[1] F. Lemeilleur et al. (ROSE Collaboration), 3rd RD48 status report, R&D on silicon for future experiments, CERN-LHCC-2000-009, Geneva, December 1999

[2] M. S. Alam *et al.*, "The ATLAS silicon pixel sensors", Nucl. Instr. & Meth. A **456** (2001) 217

[3] R. Wunstorf, "Radiation tolerant sensors for the ATLAS pixel detector", Nucl. Instr. & Meth. A **466** (2001) 327

[4] G. Lindström *et al.*, "Radiation hard silicon detectors developments by the RD48 collaboration" Nucl. Instr. & Meth. A **466** (2001) 308

[5] J. Wüstenfeld, "Characterisation of ionisation-induced surface effects for the optimisation of silicon-detectors for particle physics applications", PhD thesis, University of Dortmund, August 2001
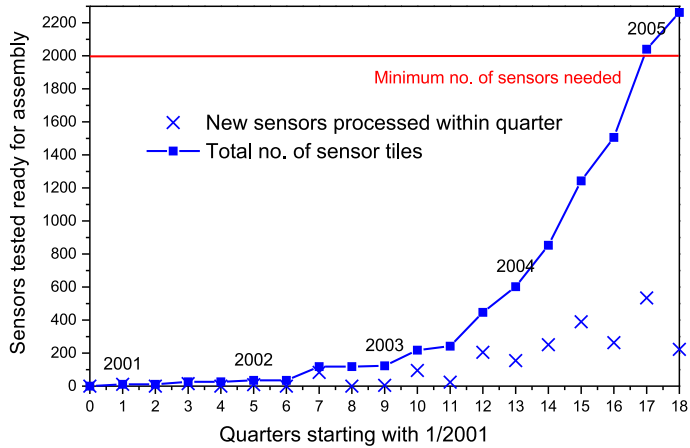
Figure 9: Sensor tile output in sum and per quarter for all ATLAS pixel laboratories in total during the production process

[6] R. H. Richter, "Radiation tolerance of detectors with p-spray isolation", presented at the 9th European Symposium on Semiconductor Detectors, Elmau/Germany, June 2002

[7] I. Gorelov *et al.*, "Electrical characteristics of silicon pixel detectors", Nucl. Instr. & Meth. A **489** (2002) 202

[8] J. M. Klaiber-Lodewigs, "Pixel Sensor Quality Assurance Plan", ATLAS Project Document ATL-IP-QA-0001, CERN 2004

[9] J. M. Klaiber-Lodewigs, "Evaluation of testing strategies for the radiation tolerant ATLAS n^+-in-n pixel sensor", Nucl. Instr. & Meth. A**512** (2003) 332

[10] J. M. Klaiber-Lodewigs, "The ATLAS Pixel Sensor — protperties, characterization and quality control", PhD thesis, University of Dortmund, 2005

[11] L. Rossi, "Pixel detectors hybridisation", Nucl. Instr. & Meth. A **501** (2003) 239